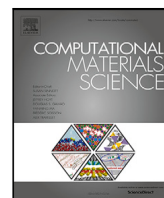| Title	Energetical effects of the edges and vertices of face-centered-cubic Pd and Au nanoparticles: A density functional theory study
Author(s)	Ishii, Akio
Citation	Computational Materials Science. 2024, 243, p. 113122
Version Type	VoR
URL	https://hdl.handle.net/11094/95743
rights	This article is licensed under a Creative Commons Attribution-NonCommercial-NoDerivatives 4.0 International License.
Note	

Contents lists available at ScienceDirect

Computational Materials Science

Full length article

Energetical effects of the edges and vertices of face-centered-cubic Pd and Au nanoparticles: A density functional theory study

Akio Ishii

Department of Mechanical Science and Bioengineering, Osaka University, 1-3 Machikaneyama-cho, Toyonaka, Osaka 560-8531, Japan

ARTICLE INFO

ABSTRACT

The properties of nanoparticles depend on their sizes, and these size effects in face-centered-cubic (FCC) nanoparticles are attributed to the edge and vertex effects. However, the effects of edges and vertices on the properties of nanoparticles have not yet been explicitly investigated. In this study, we propose a method to evaluate the edge and vertex effects in FCC nanoparticles using density functional theory atomistic simulations. Pd and Au FCC nanoparticles are modeled as conventional truncated octahedra with {111} and {100} faces. The changes in the excess energy due to the edges and vertices are separately described and are calculated with respect to the size of the nanoparticles. Through explicit calculations, we confirmed that for Pd and Au nanoparticles with several hundred atoms, the vertex effects are negligible, whereas the edge effects are still significant.

1. Introduction

Nanoparticles exhibit unique properties that depend on their shape and size. In particular, the properties of small nanoparticles differ from those of large nanoparticles and bulk metals [1–11]. The properties of nanoparticles have been extensively investigated to develop nanoparticles with desirable characteristics [12–14]. The metals Pd, Pt, Au and Ag have been conventionally used to prepare nanoparticles because they exhibit high stabilities [15,16]. These metals usually have face-centered-cubic (FCC) crystal structures and FCC nanoparticles have truncated octahedral structures with {111} (hexagons) and {100} faces (tetragons) as stable shapes [11,17,18]. Apart from the {111} and {100} faces, the edges between {111} and another {111} planes ({111}/{111}), {111} and {100} planes ({111}/{100}) and the vertices between {111}, {100} and another {111} planes are geometrically necessary to construct such octahedral nanoparticles. Hence, the size effect in such FCC nanoparticles can reasonably be attributed to the edges and vertices of the octahedra. Nevertheless, the effects of edges and vertices on the properties of nanoparticles have not yet been explicitly investigated and they remain unclear because of the lack of a methodological study to examine the effect. To understand such effect is useful in understanding the thermodynamic and mechanical stability of crystals and it is also connected to the nucleation of extended defect such as dislocations in nano-scale metals, which is informative to the mechanical properties.

In this study, we propose a method to evaluate the energetical effects of the edges and vertices of FCC nanoparticles using density functional theory (DFT) atomistic simulations. We model Pd and Au FCC nanoparticles as conventional truncated octahedra with {111} and {100} faces. The changes in excess energy due to the edges and vertices are separately described and calculated with respect to the size of nanoparticles. In the following sections, we simply denote the excess energies as "edge" and "vertex" energies.

2. Calculation of the edge energy

First, we calculated the edge energy of the conventional truncated octahedral FCC nanoparticle with {111} and {100} faces using a 2D atomic model. A schematic of the 2D atomic model used herein is shown in Fig. 1. The 2D model is a hexagonal prism with {111}/{111} and {111}/{100} edges and an infinite length along the longitudinal direction z. Herein, a_z^{2D}, the thickness of the unit cell along the z direction, is very small owing to the periodicity along the z direction. The {111}/{111} and {111}/{100} edges correspond to those of the conventional truncated octahedral FCC nanoparticle but no vertices exist owing to the periodicity along z direction in this model. Thus, we distinguish between the effects of edges and the effects of vertices and the edge energy of the nanoparticle is defined as follows:

$$\Delta E^{\mathrm{edge}} \equiv \frac{1}{a_z^{\mathrm{2D}}} \left(E^{\mathrm{2D}} - N^{\mathrm{2D}} E^{\mathrm{bulk}} - \gamma^{\{111\}} A_{\{111\}}^{\mathrm{2D}} - \gamma^{\{100\}} A_{\{100\}}^{\mathrm{2D}} \right). \quad (1)$$

Here, E^{2D} denotes the potential energy of the 2D atomic model for the optimized atomic structures calculated via DFT; E^{bulk} denotes the
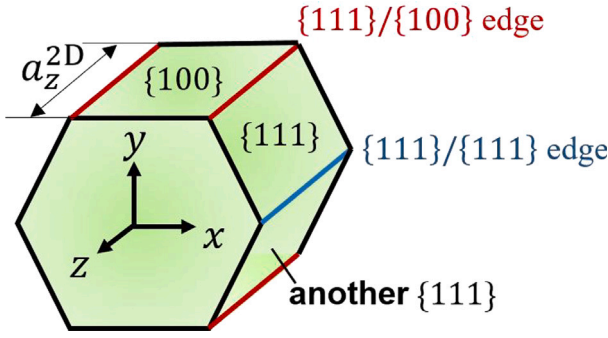
E-mail address: ishii@me.es.osaka-u.ac.jp.

Fig. 1. The schematic of 2D atomic model (hexagonal prism shape). The atomic model has periodicity (infinite length) *only* along z direction.

Table 1
Bulk energy and surface energy for orientations {111} and {100} of the FCC structure of Pd and Au, calculated using DFT atomistic simulations, those were derived from the Materials Project database [22].

	Pd	Au
E^{bulk} (eV/atom)	−5.22	−3.22
$\gamma^{\{111\}}$ (J/m²)	1.34	0.710
$\gamma^{\{100\}}$ (J/m²)	1.52	0.861

Table 2
Calculated edge energy ΔE^{edge} with respect to the number of the atom of 2D atomic models in Fig. 2. The unit is eV/Å.

N^{2D}	Pd	Au
14	0.910	0.545
19	0.912	0.528
24	0.933	0.489
29	0.933	0.485
34	0.937	0.487

Fig. 2. 2D atomic models with different distance between {111}/{100} edges to check the convergence of ΔE^{edge}. The thickness of the unit cell along z direction is two ($\bar{1}10$) atomic layers for all models. The atomic structures are visualized using the OVITO software [23].

Table 3
Calculated edge energy ΔE^{edge} with respect to the number of the atom of 2D atomic models in Fig. 3. The unit is eV/Å. The value of $N^{\text{2D}} = 29$ model in Table 2 is also listed as an reference.

N^{2D}	Pd	Au
29	0.933	0.485
44	0.933	0.500
61	0.929	0.491

bulk energy (per atom) of the materials without any surfaces; $\gamma^{\{111\}}$ and $\gamma^{\{100\}}$ denote the surface energies of the {111} and {100} faces, respectively; N^{2D} denotes the number of atoms in the 2D atomic model; and $A^{\text{2D}}_{\{111\}}$ and $A^{\text{2D}}_{\{100\}}$ denote the surface areas of {111} and {100} in the 2D atomic model.

To verify the convergence of the edge energy ΔE^{edge} with respect to the size of the atomic models for Pd and Au, we first constructed atomic models with different distances between the {111}/{100} edges as shown in Fig. 2, and the ΔE^{edge} for these models were calculated. The Vienna Ab initio Simulation Package was used for the DFT atomistic simulations [19]. The electron–ion interactions were described using the projector-augmented wave method [20]. The exchange–correlation between the electrons was treated using the Perdew–Burke–Ernzerhof generalized gradient approximation [21] with an energy cutoff of 520 eV for the plane-wave basis set. The energy convergence criteria for the electronic and ionic structure relaxations were set to 1.0×10^{-6} and 1.0×10^{-3} eV, respectively. A $1 \times 1 \times 8$ k-point mesh was used. The size of the supercell was set to $50 \times 50 \times a^{\text{2D}}_z$ Å to describe the vacuum around the faces on xy plane. E^{2D} for each atomic model was calculated after structural optimization (including the cell length along z direction). The values of E^{bulk}, $\gamma^{\{111\}}$, and $\gamma^{\{100\}}$, obtained from the Materials Project database [22], are listed in Table 1. Table 2 lists the calculated ΔE^{edge} values for each atomic model. The results show that the value of the edge energy converged at $N^{\text{2D}} = 24$, and the energy difference was lower than 10^{-2} eV/Å. Thus, the range of the interaction between the edges is a mere six {110} atomic layers.

The convergence of ΔE^{edge} for the {111}/{100} edges was confirmed. Next, we examined the convergence for the {111}/{100} edges. Based on the atomic models with $N^{\text{2D}} = 29$ in Fig. 2, which ΔE^{edge} is converged, we constructed two atomic models with different distance

between {111}/{111} edges as in Fig. 3 and the edge energies were calculated. Note that the settings of DFT calculation, including the size of the supercell, are same as those we previously mentioned in this section. The results are presented in Table 3. The difference in ΔE^{edge} for $N^{\text{2D}} = 44$ and $N^{\text{2D}} = 61$ was small, and we believe that ΔE^{edge} converged with respect to the distance between the {111}/{111} edges. Hence, the converged ΔE^{edge} values for Pd and Au were determined as 0.93 and 0.49 eV/Å. The value of ΔE^{edge} calculated in this section may not be physically very important because it includes the information on both the {111}/{111} and {111}/{100} edges due to the settings of 2D atomic model. A more practical calculation of the edge energy of the nanoparticle is presented in the appendix, wherein the edge energy is calculated separately for the {111}/{111} and {111}/{100} edges.

3. Calculation of the vertex energy

Once ΔE^{edge} was calculated, we calculated the vertex energy ΔE^{vertex} using the atomic model of an actual truncated octahedral FCC nanoparticle with identical edge lengths a. Fig. 4 shows a schematic of our 2D atomic model which corresponds to the model with 2 {111}/{111} and 4 {111}/{100} edges from the nanoparticle, which have 12 {111}/{111} and 24 {111}/{100} edges. Thus, the vertex energy ΔE^{vertex}, which corresponds to the effect of the vertex, can be obtained from the potential energy of nanoparticle E^{nanoP} and calculated ΔE^{edge} to cancel
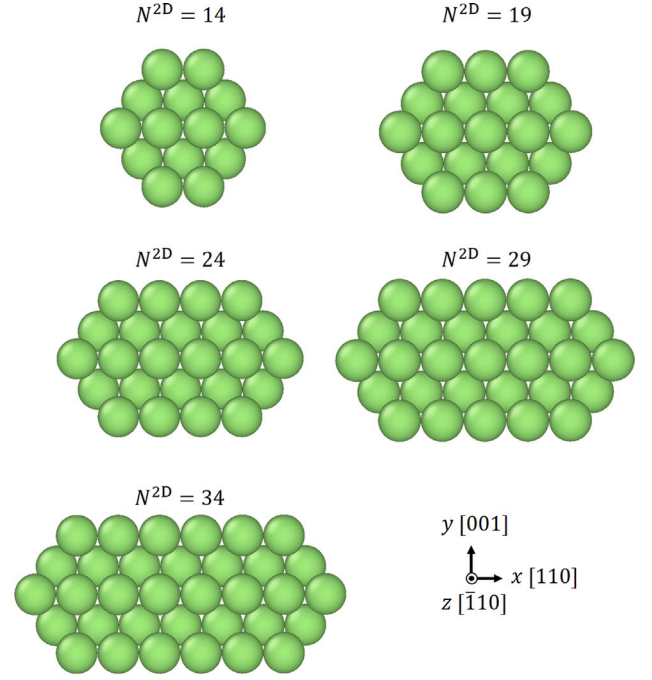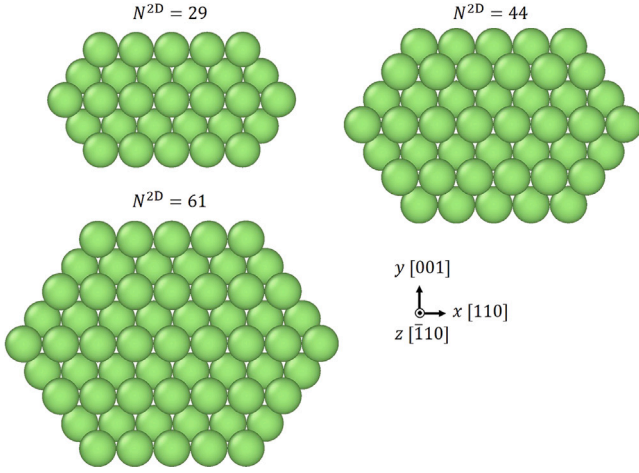
Fig. 3. 2D atomic models with different distance between {111} edges to examine the convergence of ΔE^{edge}. The thickness of the unit cell along z direction is two $(\bar{1}10)$ atomic layers for all models. The atomic model of $N^{2D} = 29$ in Fig. 2 is also shown as an reference. The atomic structures are visualized using the OVITO software [23].

Fig. 4. The relationship between the 2D atomic model and the truncated octahedral FCC nanoparticle with the identical length a for all edges. The broken lines indicated the hidden edges from the viewpoint.

the edge effect:

$$\Delta E^{\text{vertex}} \equiv \frac{1}{24}\left(E^{\text{nanoP}} - N^{\text{nanoP}} E^{\text{bulk}} - 6\Delta E^{\text{edge}} a - \left(12\sqrt{3}\gamma^{\{111\}} + 6\gamma^{\{100\}} \right) a^2 \right). \tag{2}$$

Here, N^{nanoP} denotes the number of atoms in the nanoparticle; $12\sqrt{3}a^2$ and $6a^2$ indicate the total areas of the {111} and {100} faces of the truncated octahedron, respectively; and 24 corresponds to the number of vertices in the truncated octahedron.

We constructed three atomic models with different sizes, as shown in Fig. 5, to investigate the size effect of the nanoparticles. Note only the three atomic structures in Fig. 5 are possible as truncated octahedral FCC nanoparticles with {111} and {100} faces and same length of edges in the calculatable size using our computational resource. The converged ΔE^{edge} values obtained in the previous section were used. That is, in this calculation, the size effect of the nanoparticle was considered to correspond to the change in the vertex energy ΔE^{vertex}. Moreover, the k-point mesh was changed to $1 \times 1 \times 1$, and the size of the supercell was set to $50 \times 50 \times 50$ Å to describe the vacuum around the nanoparticle; no periodicity was assumed in the atomic models of the nanoparticles.

Table 4 lists the calculated vertex energies ΔE^{vertex} with respect to the size of the nanoparticle. The value of ΔE^{vertex} decreased with an increase in the nanoparticle size. Table 5 shows the percentages of the surface, edge, and vertex energies that contribute to the total excess energy of the nanoparticle (the energy increment from the bulk FCC). Although the effect of the vertex energy ΔE^{vertex} on Pd was minimal (less than 10%), the effect of vertex energy was significant for small Au nanoparticles. For the large nanoparticle with 500 atoms, the vertex energy ΔE^{vertex} was largely negligible for both nanoparticles. However, the edge effect was significant: the edge energy ΔE^{edge} accounted for 20% of the excess energy. In this calculation, the change in the vertex energy with respect to N^{nanoP} was considered to correspond to the size effect of the nanoparticle. Hence, we conclude that the size effect is negligible for Pd and Au nanoparticles with more than 200 atoms wherein the vertex energy ΔE^{vertex} accounted for less than 10% of the excess energy. We think that our result is consistent with the experimental observation of spherical shape for the nanoparticles with the relatively large size [2,24]. Because many edges and vertices
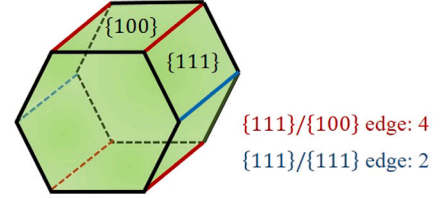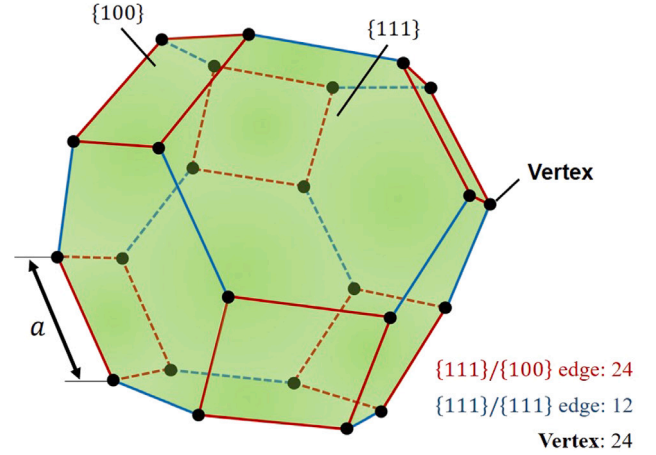
Table 4
Calculated vertex energy ΔE^{vertex} with respect to the number of the atom in nanoparticle in Fig. 5. The unit is eV (per vertex).

N^{nanoP}	Pd	Au
38	0.137	0.228
201	0.102	0.204
586	0.056	0.168

are necessary to construct spherical nanoparticles, this indicates that the excess energies due to edges and vertices become very small or negligible for the large nanoparticle. Note we also implemented the calculation of edge and vertex energies using preexisting empirical and machine learning potentials in our appendix to investigate the size effect of edge and vertex energies for larger nanoparticles and the validity of such potentials for the analysis of nanoparticles. From the result, we think the accuracy of the present empirical potentials may be not enough to calculate edge and vertex energy.

4. Conclusion

In this study, we proposed a method to evaluate the energetical effects of the edges and vertices of FCC nanoparticles using DFT atomistic simulations. Pd and Au nanoparticles were modeled as FCC nanoparticles with conventional truncated octahedra with {111} and {100} faces. The changes in the excess energy due to the edges and vertices were described separately and were calculated with respect to the size of the nanoparticles. We confirmed through explicit calculations that
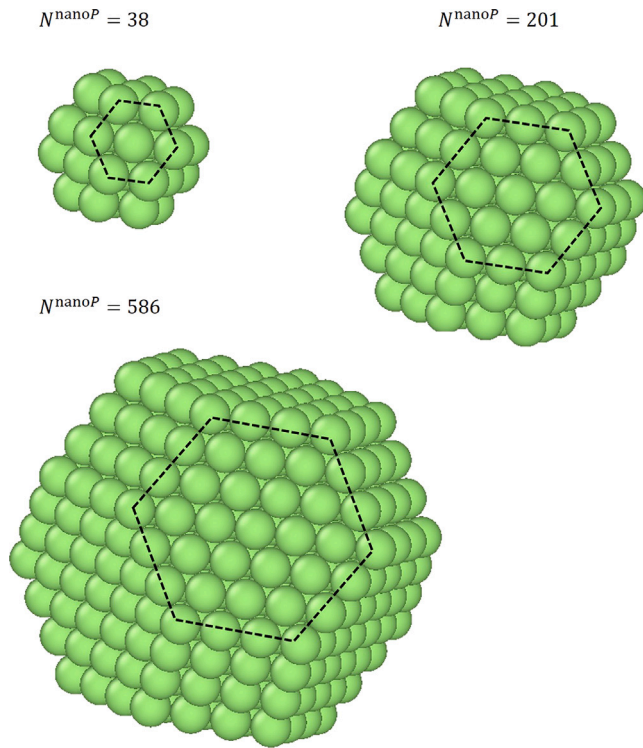
Fig. 5. Atomic models of the nanoparticles with different size for the calculation of ΔE^{vertex}. Broken lines are the guides of the eyes for a certain {111} face. The atomic structures are visualized using the OVITO software [23].

Table 5
The fraction of surface, edge and vertex energy in the total excess energy of the nanoparticle. The unit is %.

N^{nanoP}	Surface	Edge	Vertex
Pd			
38	48	43	9
201	68	30	2
586	77	23	Lower than 1
Au			
38	42	35	23
201	65	27	8
586	76	21	3

Table A.1
Calculated edge energies for {111}/{111} and {111}/{100}. The unit is eV/Å.

	Pd	Au
$\Delta E^{\text{edge}}_{\{111\}/\{111\}}$	0.201	0.166
$\Delta E^{\text{edge}}_{\{111\}/\{100\}}$	0.131	0.039

the vertex effects were negligible for Pd and Au nanoparticles with several hundred atoms, although the edge effects were still significant.

Our approach is also applicable to the calculation of the energies for edges and vertices of nanovoids (or bubbles) [25] and coherent nano inclusions [26–28]. Once the edge and vertex energies are obtained, it is useful to give the energetics to larger-scale computational simulation, such as phase-field or other micromechanics-based meso-scale simulations [29–32]. These large-scale simulations are usually limited by the

chemical interfacial energy obtained in atomistic simulations. Thus, our approach can help achieve parameter-free multi-scale computational analysis, and these aspects will be considered in future studies.

CRediT authorship contribution statement

Akio Ishii: Writing – review & editing, Writing – original draft, Visualization, Software, Resources, Methodology, Investigation, Funding acquisition, Formal analysis, Conceptualization.

Declaration of competing interest

The authors declare that they have no known competing financial interests or personal relationships that could have appeared to influence the work reported in this paper.

Data availability

Data will be made available on request.

Acknowledgments

Appendix A. The dissolution of the edge energy to {111}/{111} and {111}/{100} edges

The edge energy can be separated into $\Delta E^{\text{edge}}_{\{111\}/\{111\}}$ (corresponding to the {111}/{111} edge) and $\Delta E^{\text{edge}}_{\{111\}/\{100\}}$ (corresponding to the {111}/{100} edge). This can be achieved using the calculated ΔE^{edge} and ΔE^{vertex} values and E^{nanoP2}. Here, E^{nanoP2} denotes the potential energy of the truncated octahedral FCC nanoparticle with different edge lengths for {111}/{111} and {111}/{100} ($a_{\{111\}/\{111\}}$ and $a_{\{111\}/\{100\}}$), as shown in Fig. A.1. Compared with the edge energy of nanoparticles with identical length of the edges $a_{\{111\}/\{100\}}$, the excess edge energy for {111}/{111} exists in the nanoparticle in Fig. A.1 due to the difference between the lengths of {111}/{111} and {111}/{100} edges. Thus, $\Delta E^{\text{edge}}_{\{111\}/\{111\}}$ and $\Delta E^{\text{edge}}_{\{111\}/\{100\}}$ can be derived as following:

$$\Delta E^{\text{edge}}_{\{111\}/\{111\}} = \frac{1}{12(a_{\{111\}/\{111\}} - a_{\{111\}/\{100\}})}$$
$$\times \left(E^{\text{nanoP2}} - N^{\text{nanoP2}} E^{\text{bulk}} - 24\Delta E^{\text{vertex}} \right.$$
$$\left. - 6\Delta E^{\text{edge}} a_{\{111\}/\{100\}} - \gamma^{\{111\}} A^{\text{nanoP2}}_{\{111\}} - \gamma^{\{100\}} A^{\text{nanoP2}}_{\{100\}} \right),$$
$$\Delta E^{\text{edge}}_{\{111\}/\{100\}} = \frac{1}{24} \left(\Delta E^{\text{edge}} - 12\Delta E^{\text{edge}}_{\{111\}/\{111\}} \right). \quad (A.1)$$

Here, N^{nanoP2} denotes the number of atoms in the nanoparticle; $A^{\text{nanoP2}}_{\{111\}}$ and $A^{\text{nanoP2}}_{\{100\}}$ denote the total areas of the {111} and {100} faces of the nanoparticle, respectively; the numbers of the {111}/{111} edges, {111}/{100} edges, and vertices of the nanoparticle are 12, 24 and 24, respectively. The values of ΔE^{vertex} for $N^{\text{nanoP}} = 586$ nanoparticles were used in the calculations. Although a larger nanoparticle may help to reduce the size effect and examine the convergence of the edge energy, we only calculated the edge energy for $N^{\text{nanoP2}} = 314$ nanoparticle in Fig. A.1 due to computational limitations; we emphasize here that an atomic model with $N^{\text{nanoP2}} = 314$ is very large for conventional DFT calculations. The settings of DFT calculation, including the size of the supercell, are same as those in Section 3. The results are listed in Table A.1. The value of $\Delta E^{\text{edge}}_{\{111\}/\{100\}}$ is usually smaller than that of $\Delta E^{\text{edge}}_{\{111\}/\{111\}}$. We believe this is because the angle between {111} and {100} faces is obtuse though that between {111} and {111} faces is acute.

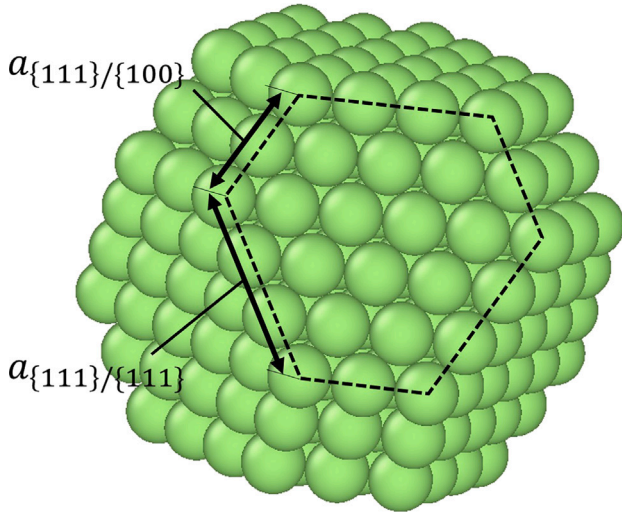**Fig. A.1.** The atomic model of the nanoparticle with different length of the edges of {111}/{111} and {111}/{100} for the dissolution of edge energy ($N^{\text{nanoP2}} = 314$). Broken lines are the guides of the eyes for a certain {111} face. The atomic structures are visualized using the OVITO software [23].

Appendix B. Calculation of the edge and vertex energies using empirical and machine learning potentials

To investigate the size effect of edge and vertex energies and the validity of preexisting empirical and machine learning potentials (MLP) for the analysis of nanoparticles, we also implemented the calculation of edge and vertex energies using such potentials. For the calculation of edge energy, addition to $N^{\text{2D}} = 14$ model in Fig. 2, we prepared four 2D hexagonal prism atomic models with different size: $N^{\text{2D}} = 43$, 149, 319 and 694 as in Fig. B.1. For the calculation of vertex energy, addition to $N^{\text{2D}} = 201$ and 586 models in Fig. 5, we prepared three truncated octahedral FCC nanoparticles with identical edge lengths, which have different size: $N^{\text{nanoP}} = 1289$, 4033 and 9201 as in Fig. B.2. Molecular statics simulation (structure relaxation) was implemented using LAMMPS code [33]. For both Pd and Au nanoparticles, Shan *et al.* embedded atom method (EAM) potential [34,35] and Seko's polynominal MLP [36] were used, respectively. The energy tolerance for the convergence of the structure relaxation of LAMMPS code was set to 1.0×10^{-10}.

First, we show the calculated bulk and surface energies for each potentials in Table B.1. Here we do not explain the detail of the method to calculate surface energy because it already becomes common [37]. Although the difference between the surface energies are small, the EAM potential seems to reproduce the trend of the DFT calculation. On the other hand, we confirmed MLP suffers from the reproduction of the DFT result; the negative surface energies are calculated for Au as in Table B.1. And even for Pd case, we confirmed the calculated edge energies using MLP becomes negative and the hexagonal structures of the 2D atomic models collapsed during the relaxation, e.g., $\Delta E^{\text{edge}} = -1.25$ eV/Å for $N^{\text{2D}} = 149$ model. We think this is because the training for the heterogeneous structures are not enough. In Tables B.2 and B.3, the calculated edge and vertex energies using the EAM potentials are shown. Although the values are positive, both edge and vertex energies did not converge and tend to increase with respect to the size of atomic models. As we discussed in Section 3, this is not consistent with the experimental observation [2,24] and unrealistic. Note $\Delta E^{\text{edge}} = 0.40$ and 0.24 eV/Å were used for Pd and Au representatively for the calculation of the vertex energy because the edge energies did not converge. Eventually, we concluded the accuracy of the EAM potential and MLP are not enough to calculate edge and vertex energy.
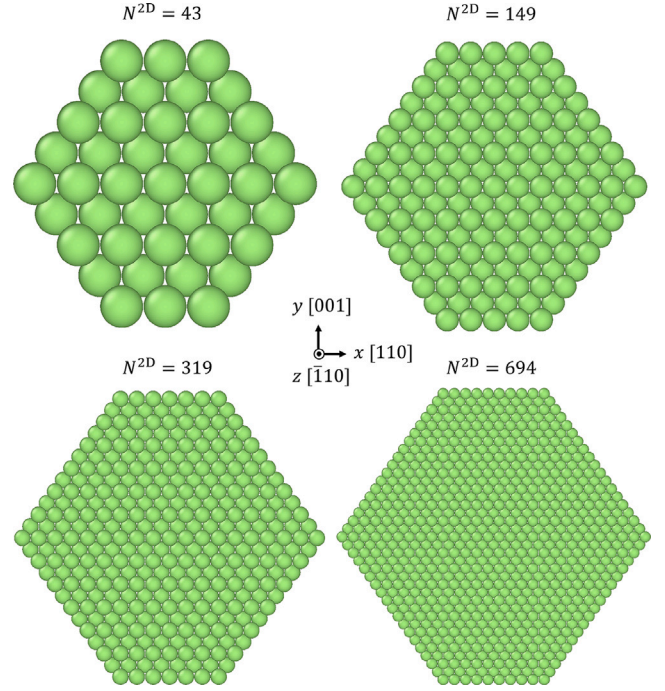

Fig. B.1. 2D atomic models with different size for the calculation of ΔE^{edge} using empirical and machine learning potentials. The thickness of the unit cell along z direction is two ($\bar{1}10$) atomic layers for all models. The atomic structures are visualized using the OVITO software [23].

Table B.1
Calculated bulk energy and surface energy for orientations {111} and {100} of the FCC structure of Pd and Au using EAM potential [34,35] and MLP [36].

	Pd	Au
EAM		
E^{bulk} (eV/atom)	−2.76	−2.40
$\gamma^{\{111\}}$ (J/m^2)	0.60	0.33
$\gamma^{\{100\}}$ (J/m^2)	0.67	0.36
MLP		
E^{bulk}	−3.75	−3.04
$\gamma^{\{111\}}$	1.26	−0.88
$\gamma^{\{100\}}$	1.72	−0.73

Table B.2
Calculated edge energy ΔE^{edge} with respect to the number of the atom of 2D atomic models using EAM potentials. The unit is eV/Å.

N^{2D}	Pd	Au
14	0.404	0.231
43	0.400	0.241
149	0.402	0.244
319	0.417	0.250
694	0.446	0.262

Table B.3
Calculated vertex energy ΔE^{vertex} with respect to the number of the atom in nanoparticle using EAM potentials. The unit is eV (per vertex).

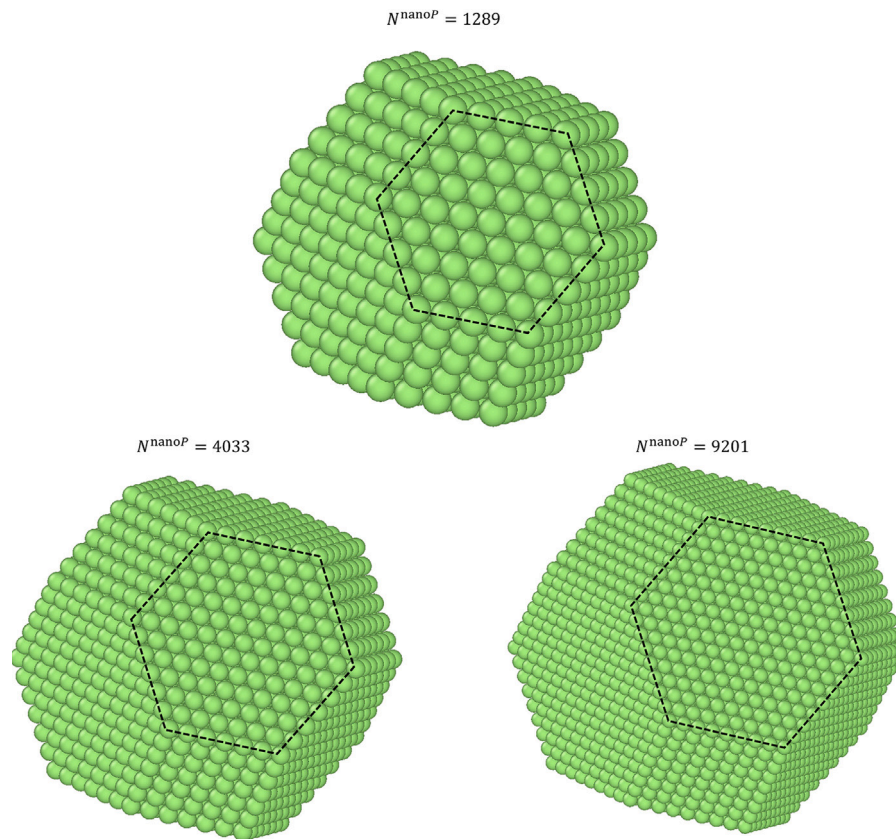| N^{nanoP}	Pd	Au
201	0.101	0.068
586	0.133	0.092
1289	0.152	0.100
4033	0.245	0.134
9201	0.307	0.187

Fig. B.2. Atomic models of the nanoparticles with different size for the calculation of ΔE^{vertex} using empirical and machine learning potentials. Broken lines are the guides of the eyes for a certain {111} face. The atomic structures are visualized using the OVITO software [23].

References

[1] H.R. Stuart, D.G. Hall, Island size effects in nanoparticle-enhanced photodetectors, Appl. Phys. Lett. 73 (1998) 3815–3817.

[2] R. Narayanan, M.A. El-Sayed, Catalysis with transition metal nanoparticles in colloidal solution: Nanoparticle shape dependence and stability, J. Phys. Chem. B 109 (2005) 12663–12676.

[3] A. Albanese, P.S. Tang, W.C. Chan, The effect of nanoparticle size, shape, and surface chemistry on biological systems, Annual Rev. Biomed. Eng. 14 (2012) 1–16.

[4] X.H. Liu, L. Zhong, S. Huang, S.X. Mao, T. Zhu, J.Y. Huang, Size-dependent fracture of silicon nanoparticles during lithiation, ACS Nano 6 (2012) 1522–1531.

[5] J. Zheng, C. Zhou, M. Yu, J. Liu, Different sized luminescent gold nanoparticles, Nanoscale 4 (2012) 4073.

[6] M. Settem, R. Ferrando, A. Giacomello, Tempering of Au nanoclusters: Capturing the temperature-dependent competition among structural motifs, Nanoscale 14 (2022) 939–952.

[7] M. Settem, C. Roncaglia, R. Ferrando, A. Giacomello, Structural transformations in Cu, Ag, and Au metal nanoclusters, J. Chem. Phys. 159 (2023) 094303.

[8] S.G. Lambie, G.R. Weal, C.E. Blackmore, R.E. Palmer, A.L. Garden, Contrasting motif preferences of platinum and gold nanoclusters between 55 and 309 atoms, Nanoscale Adv. 1 (2019) 2416–2425.

[9] H. Xu, M. Molayem, M. Springborg, Theoretical study of the structural and energetic properties of platinum clusters with up to 60 atoms, Str. Chem. 32 (2021) 469–479.

[10] D. Nelli, Central vacancy creation in icosahedral nanoparticles induced by the displacement of large impurities, Eur. Phys. J. Appl. Phys. 97 (2022) 18.

[11] A. Ishii, N. Nakamura, Ab initio morphology prediction of Pd, Ag, Au, and Pt nanoparticles on (0001) sapphire substrates, J. Appl. Phys. 135 (2024) 094301.

[12] C.M. Welch, R.G. Compton, The use of nanoparticles in electroanalysis: a review, Anal. Bioanal. Chem. 384 (2006) 601–619.

[13] V. Mohanraj, Chen, Nanoparticles-a review, Trop. J. Pharm.l Res. 5 (2006) 561–573.

[14] R. Ferrando, J. Jellinek, R.L. Johnston, Nanoalloys: From theory to applications of alloy clusters and nanoparticles, Chem. Revi. 108 (2008) 845–910.

[15] N. Nakamura, K. Matsuura, A. Ishii, H. Ogi, Restructuring in bimetallic core-shell nanoparticles: Real-time observation, Phys. Rev. B 105 (2022) 125401.

[16] N. Nakamura, K. Matsuura, A. Ishii, In situ observation of morphological change of Pd-based bimetallic nanoparticles synthesized by co-sputtering, J. Appl. Phys. 134 (2023) 145301.

[17] G.D. Barmparis, Z. Lodziana, N. Lopez, I.N. Remediakis, Nanoparticle shapes by using Wulff constructions and first-principles calculations, Beil. J. Nanotech. 6 (2015) 361–368.

[18] S. Divi, A. Chatterjee, Generalized nano-thermodynamic model for capturing size-dependent surface segregation in multi-metal alloy nanoparticles, RSC Adv. 8 (2018) 10409–10424.

[19] G. Kresse, J. Furthmüller, Efficient iterative schemes for ab initio total-energy calculations using a plane-wave basis set, Physi. Rev. B 54 (1996) 11169–11186.

[20] G. Kresse, D. Joubert, From ultrasoft pseudopotentials to the projector augmented-wave method, Phys. Rev. B 59 (1999) 11–19.

[21] J. Perdew, K. Burke, M. Ernzerhof, Generalized gradient approximation made simple, Phys. Rev. Lett. 77 (1996) 3865–3868.

[22] A. Jain, S.P. Ong, G. Hautier, W. Chen, W.D. Richards, S. Dacek, S. Cholia, D. Gunter, D. Skinner, G. Ceder, et al., Commentary: The materials project: A materials genome approach to accelerating materials innovation, APL Mater. 1 (2013) 011002.

[23] A. Stukowski, Visualization and analysis of atomistic simulation data with OVITO-the open visualization tool, Model. Sim. Mater. Sci. Eng. 18 (2010) 015012.

[24] Y. Li, Q. Liu, W. Shen, Morphology-dependent nanocatalysis: Metal particles, Dalton Trans. 40 (2011) 5811–5826.

[25] W. Geng, L. Wan, J.-P. Du, A. Ishii, N. Ishikawa, H. Kimizuka, S. Ogata, Hydrogen bubble nucleation in α-iron, Scr. Mater. 134 (2017) 105–109.

[26] H. Miyoshi, H. Kimizuka, A. Ishii, S. Ogata, Temperature-dependent nucleation kinetics of Guinier-Preston zones in Al–Cu alloys: An atomistic kinetic Monte Carlo and classical nucleation theory approach, Acta Mater. 179 (2019) 262–272.

[27] H. Miyoshi, H. Kimizuka, A. Ishii, S. Ogata, Competing nucleation of single- and double-layer Guinier–Preston zones in Al–Cu alloys, Sci. Rep. 11 (2021) 4503.

[28] H. Liao, H. Kimizuka, A. Ishii, J.-P. Du, S. Ogata, Nucleation kinetics of the β'' precipitate in dilute Mg–Y alloys: A kinetic Monte Carlo study, Scr. Mater. 210 (2022) 114480.

[29] A. Ishii, Energetics of heterogeneous Mg $\{10\bar{1}2\}$ deformation twinning migration using an atomistically informed phase-field model, Comput. Mater. Sci. 183 (2020) 109907.

[30] A. Ishii, *Ab* Initio morphology prediction of Zr hydride precipitates using atomistically informed Eshelby's ellipsoidal inclusion, Comput. Mater. Sci. 211 (2022) 111500.

[31] A. Ishii, Influence of elastic anisotropy on the shapes of ellipsoidal blisters and stress field around the blisters in solid materials, AIP Adv. 13 (2023) 125024.

[32] A. Ishii, Morphology prediction of elastically interacting Zr hydride precipitates and cracks in α-Zr using atomistically informed Eshelby's ellipsoidal inclusion, Comput. Mater. Sci. 231 (2024) 112568.

[33] S. Plimpton, Fast parallel algorithms for short-range molecular dynamics, J. Comput. Phys. 117 (1995) 1–19.

[34] B. Shan, L. Wang, S. Yang, J. Hyun, N. Kapur, Y. Zhao, J.B. Nicholas, K. Cho, First-principles-based embedded atom method for PdAu nanoparticles, Phys. Rev. B 80 (2009) 035404.

[35] B. Shan, L. Wang, S. Yang, J. Hyun, N. Kapur, Y. Zhao, J.B. Nicholas, K. Cho, Erratum: First-principles-based embedded atom method for PdAu nanoparticles (Physical Review B - Condensed Matter and Materials Physics (2009) 80 (035404)), Phys. Rev. B 89 (2014) 159903.

[36] A. Seko, Tutorial: Systematic development of polynomial machine learning potentials for elemental and alloy systems, J. Appl. Phys. 133 (2023) 011101.

[37] R. Tran, Z. Xu, B. Radhakrishnan, D. Winston, W. Sun, K.A. Persson, S.P. Ong, Data descriptor: Surface energies of elemental crystals, Sci. Data 3 (2016) 160080.